Density profile of pyrolite under the lower mantle conditions

Angele Ricolleau, Yingwei Fei, Elizabeth Cottrell, Heather Watson, Liwei Deng, Li Zhang, Guillaume Fiquet, Anne-Line Auzende, Mathieu Roskosz, Guillaume Morard, et al.

Density profile of pyrolite under the lower mantle conditions

Angele Ricolleau,[1] Yingwei Fei,[1] Elizabeth Cottrell,[1,2] Heather Watson,[1] Liwei Deng,[1,3] Li Zhang,[1] Guillaume Fiquet,[4] Anne-Line Auzende,[4] Mathieu Roskosz,[5] Guillaume Morard,[4,6] and Vitali Prakapenka[7]

Received 25 November 2008; revised 3 February 2009; accepted 17 February 2009; published 24 March 2009.

[1] The pyrolite model is one of the possible compositions of the Earth's lower mantle. The lower mantle's composition is generally modelled by comparing seismic observations with mineral physics data of possible lower mantle end-member phases. Here, we report the compression behavior of a natural KLB-1 peridotite (a representative composition of the pyrolite model) in a quasi-hydrostatic environment at simultaneous high pressure (P) and temperature (T), covering the entire range of lower mantle P-T conditions up to 112 GPa. This is the first experimentally determined density profile of pyrolite under the lower mantle conditions. The results allow us to directly compare the measured density of peridotite mantle along the geotherm with the Preliminary Reference Earth Model (PREM) derived from seismic observations, without extrapolation. The comparison shows significant mismatch between the two, which calls for a re-evaluation of the PREM density model or a non-pyrolite lower mantle composition. **Citation:** Ricolleau, A., et al. (2009), Density profile of pyrolite under the lower mantle conditions, *Geophys. Res. Lett.*, *36*, L06302, doi:10.1029/2008GL036759.

1. Introduction

[2] There is a general consensus that the Earth's upper mantle is peridotitic (the pyrolite model), based on direct geological observations of upper mantle rocks and magmatic processes at high pressure [*Ringwood*, 1975]. A common approach to determine the composition of the lower mantle is to compare laboratory experimental data with seismic observations. The question of compositional stratification between upper and lower mantle remains open. Previous studies of the lower mantle composition were based on thermoelastic modeling of the two major phases in the lower mantle, Mg-perovskite and ferropericlase, using existing thermoelastic parameters derived from experimental data across a limited pressure and temperature range. These studies have been inconclusive, with some authors [e.g., *Jackson and Rigden*, 1996; *Stacey*, 1996] arguing that the pyrolitic composition matches the seismic data, whereas others [e.g., *Stixrude et al.*, 1992; *Murakami et al.*, 2007] disagree and propose more silicic models (a perovskitic lower mantle). None of these studies investigated a realistic multi-component mantle composition and instead drew their conclusions from a three-component system model (SiO_2-MgO-FeO). Few experiments have been carried out under lower mantle conditions for the multi-component system [*Lee et al.*, 2004; *O'Neill and Jeanloz*, 1990] but none has covered the P-T range of the entire lower mantle with high-precision data under hydrostatic conditions.

[3] In this study, we performed compression experiments on a natural KLB-1 peridotite [*Takahashi*, 1986] (similar in composition to the pyrolite model [*Ringwood*, 1975; *McDonough and Sun*, 1995]) under lower mantle pressure and temperature conditions, using synchrotron X-ray diffraction (XRD) and laser-heating diamond-anvil cell techniques. The experiments allowed us to establish a reference density profile for a peridotitic mantle and compare it to seismic observations of the lower mantle.

2. Experimental Procedure

[4] Natural KLB-1 powder was homogenized by melting at 1800°C and 1 GPa. The quenched sample contains fine melting texture with quenching crystals. It was reground, mixed with 7 wt% gold powder, and then sintered in a piston cylinder apparatus at 1 GPa and 700°C. Both piston-cylinder experiments were made using graphite capsule to keep reasonably reduced conditions, along the CCO buffer. The grain size of the recovered sample is about 1 to 2 microns and microprobe analysis showed that the composition of the sintered sample is homogeneous at a 5-μm scale, identical to the starting composition of KLB-1. The sintered samples were polished down to a thin plate with thickness between 10 and 15 μm. We loaded five diamond anvil cells (DAC) with this starting material in neon pressure transmitting medium and one cell with sodium chloride as pressure medium. *In situ* XRD patterns were collected from 30 GPa to 110 GPa and from 1400 K to 2500 K. *In situ* measurements were carried out at the GSECARS (13IDD) sector of the Advanced Photon Source (Argonne National Laboratory), and at the European Synchrotron Radiation Facility (beamline ID27). High temperature was achieved by double-sided laser-heating [*Shen et al.*, 2001]. The 20 μm laser heating spot with relatively uniform temperature was carefully aligned with a 6 μm X-ray spot to obtain diffraction data at simultaneous high P-T. Temperature measurements were acquired from both sides during each XRD acquisition. The input laser power on

[1]Geophysical Laboratory, Carnegie Institution of Washington, Washington, DC, USA.
[2]Department of Mineral Sciences, National Museum of Natural History, Smithsonian Institution, Washington, DC, USA.
[3]School of Earth and Space Sciences, Peking University, Beijing, China.
[4]Institut de Physique du Globe de Paris, IMPMC, Paris, France.
[5]Laboratoire de Structure et Proprietes de l'Etat Solide, Université des Sciences et Techniques de Lille, Villeneuve d'Ascq, France.
[6]European Synchrotron Radiation Facility, Grenoble, France.
[7]Center for Advanced Radiation Sources, University of Chicago, Argonne, Illinois, USA.

0094-8276/09/2008GL036759

Table 1. Equation of State of Mg-Perovskite, Ca-Perovskite and Ferropericlase

			Fp	
	Mg-pv	Ca-pv	HS	LS
V_0 (Å^3)	164.00 (fixed)	45.60 (fixed)	76.44 (2)	74.04 (2)
$K_{0,T}$ (GPa)	245 (1)	244 (1)	158 (fixed)	170 (fixed)
$K'_{0,T}$	4 (fixed)	4 (fixed)	4 (fixed)	4 (fixed)
$(dK/dT)_P$ ($GPaK^{-1}$)	−0.036 (1)	−0.035 (2)	−0.034 (1)	
a_0 (10^{-5} K^{-1})	3.19 (17)	3.06 (19)	2.20 (20)	
a_1 (10^{-8} K^{-2})	0.88 (16)	0.87 (18)	3.61 (27)	

each side was balanced to minimize the axial temperature gradient: the difference observed during XRD acquisition were usually less than 100 K. Data processes are described in auxiliary material[1], Figure S1. Pressures were calculated from the equation of state of gold [*Fei et al.*, 2007a]. Using neon as transmitting pressure medium provides quasi-hydrostatic pressures [*Meng et al.*, 1993]. The unit cell volumes obtained on the cell used NaCl as pressure medium are in good agreement with the others. We obtained P-V-T data from 17 XRD patterns at room temperature and 136 patterns at high temperatures up to 2569 K, covering the P-T range of the lower mantle up to 112 GPa (see Table S1).

3. Results

[5] In order to directly compare the measurements with mantle density profile derived from seismic observations, we first establish the thermal equations of state (EoS) of the three lower mantle phases (Mg-perovskite, Ca-perovskite, and ferropericlase) from our experimental data. Because the chemical compositions of these coexisting phases change slightly with the experimental P-T conditions, according to the behavior of element partitioning, the measured thermal EoS includes the effect of the chemistry change of individual phases on the measured volume, which is expected to be small (within the uncertainties of the measurements). Over the P-T range of the experiments, Mg-perovskite remains in orthorhombic structure with well resolved characteristic triplet: the 020, 112, and 200 diffraction lines (cf. Figure S1). Fitting the P-V-T data to the high-temperature Birch-Murnaghan EoS yielded parameters in Table 1 (cf. Figure S2). The EoS of the Mg-perovskite shows higher values for thermal parameters than those obtained with the $MgSiO_3$ end-member [*Fiquet et al.*, 2000]. However, the thermal behavior of our perovskite sample is similar to a recent study [*Nishiyama and Yagi*, 2007] made on a Fe- and Al-bearing Mg-perovskite which is more relevant to mantle perovskite (cf. Table S2).

[6] We observed cubic Ca-perovskite under lower mantle P-T conditions and the tetragonal structure, indicated by the splitting of the 200 peak, upon quench [e.g., *Komabayashi et al.*, 2007] (Figure S3). We refined the room-temperature volume of Ca-perovskite by a tetragonal cell with the P4/mmm space group and obtained c-axes 0.5% (±0.1%) shorter than the a-axes. All high-temperature diffraction patterns were fitted with a cubic unit cell. Because the difference of the refined volume between the cubic and tetragonal cells is negligible, the optimized parameters for Ca-perovskite (Table 1) reproduce the P-V-T data well over a large P-T range (up to 111 GPa and 2569 K) (Figure S4). The new thermal EoS of Ca-perovskite can also reproduce P-V-T data in multi-anvil experiments with a limited P-T range (up to 13 GPa and 1600 K) [*Wang et al.*, 1996].

[7] Recent measurements have showed that ferrous iron in ferropericlase undergoes a high-spin to low-spin transition over the mantle pressure range at room temperature [*Badro et al.*, 2003]. There is significant volume reduction associated with the spin transition [*Fei et al.*, 2007b]. It is still not clear if the spin transition will occur at lower mantle P-T conditions along the geotherm or how the transition will affect the mantle density profile. We have observed an abnormal volume contraction at about 50 GPa along the room-temperature compression curve which is attributed to the high-spin to low-spin transition (Figure 1). We fit our pressure-volume data at room temperature by fixing the high-spin and low-spin bulk modulus, equal to 158 GPa and 170 GPa respectively [*Fei et al.*, 2007b] (with fixed $K' = 4$), and obtained V_0 for each spin state condition (Table 1). At high temperature, we did not observe any abnormal volume contraction along the isothermal compression curve (Figure 1). The high-temperature volumes yielded the thermal parameters of ferropericlase listed in Table 1, using the room-temperature parameters of the high-spin phase. Figure 1 shows the calculated 2000 K isothermal compression curve using the thermal EoS of high-spin ferropericlase (Table 1), which reproduces the 2000-K experimental data well. Recent theoretical calculations [e.g., *Tsuchiya et al.*, 2006] predict that the spin transition at high temperature would occur continuously over a broad pressure range. Indeed, our data indicate that temperature has a strong effect on the spin transition and there is no resolvable volume change associated with the spin transition up to 110 GPa at high temperature, indicating the spin transition does not modify the density profile of the lower mantle, up to a depth of at least 2450 km.

[8] Using these newly established thermal EoS of the three lower mantle phases under mantle P-T conditions, we now calculate the densities of the individual phases using compositional information derived from phase equilibrium studies of peridotitic compositions at high pressures and temperatures in multi-anvil apparatus [*Nishiyama and Yagi*, 2003; *Wood*, 2000; *Irifune*, 1994] and in the laser-heating diamond anvil cell [*Kesson et al.*, 1998; *Murakami et al.*, 2005]. The equilibrium chemical compositions for the coexisting Mg-perovskite, Ca-perovskite, and ferropericlase phases are well established at pressures and temperatures corresponding to the top part of the lower mantle (from 660 km to 800 km) [*Nishiyama and Yagi*, 2003; *Wood*, 2000]. Assuming a constant mineral composition throughout the lower mantle, we calculated the 2000-K isotherm density profiles for Mg-perovskite, Ca-perovskite, and ferropericlase using the mineral compositions from *Nishiyama and Yagi* [2003] (Figure 2). In comparison with the PREM density model, we notice that the densities of the two perovskites match relatively well with that of PREM whereas the density of ferropericlase is significantly lower than that of PREM at the uppermost part of the lower mantle, and higher at the bottom of the mantle.

[1] Auxiliary materials are available in the HTML. doi:10.1029/2008GL036759.

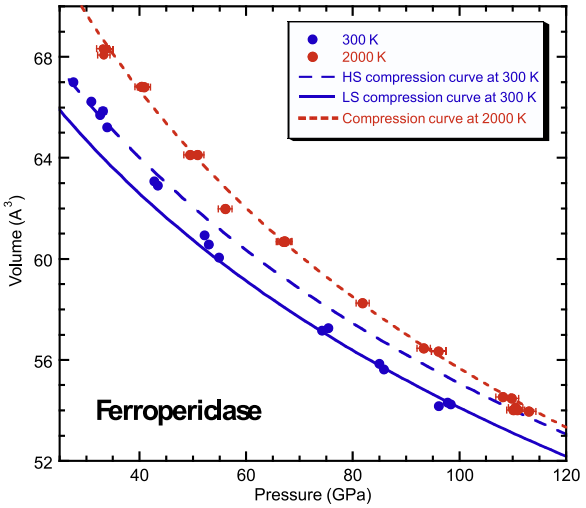

Figure 1. Pressure-volume relationship of ferropericlase at 300 K (blue circles) and at 2000 K (±50 K) (red circles). The dashed and solid blue curves, and the dashed red curve are the compression curves obtained with the equation of state of ferropericlase (Table 1), at room temperature for high-spin and low-spin, and at 2000 K, respectively. The ferropericlase in KLB-1 starting composition contains about 15 atom% iron. However, the data can be reproduced by the equation of state of $(Mg_{0.80}, Fe_{0.20})O$ [*Fei et al.*, 2007b]. This larger volume than expected could be explained by the presence of minor elements in the KLB-1 ferropericlase, such as Ni, Cr and Na, which enter ferropericlase preferentially [*Irifune*, 1994].

[9] To compare the PREM model to our measured KLB-1 mantle density profile in detail, we examine the effect of mineral composition change on the density profiles as a function of depth. Because the composition of Ca-perovskite remains relatively constant throughout the lower mantle [*Kesson et al.*, 1998], the compositional effect from Ca-perovskite is negligible. On the other hand, the changing Fe-Mg partition coefficient between Mg-perovskite and ferropericlase as a function of depth [*Mao et al.*, 1997] could influence the calculated density profiles. The measured Fe-Mg partition coefficients ($K_D = X^{pv}_{Fe}X^{fp}_{Mg}/X^{pv}_{Mg}X^{fp}_{Fe}$) vary from 0.4 to 1.2 [*Nishiyama and Yagi*, 2003; *Wood*, 2000; *Irifune*, 1994; *Kesson et al.*, 1998; *Murakami et al.*, 2005] (Figure S5). We chose sets of Mg-perovskite and ferropericlase compositions [*Nishiyama and Yagi*, 2003; *Wood*, 2000; *Kesson et al.*, 1998] obtained on pyrolitic composition, giving the iron bulk molar fraction, i.e. X_{Fe} = Fe/(Fe + Mg), of 0.106, consistent with the mantle model of *McDonough and Sun* [1995]. We then computed mineral proportions in the assemblage based on mass balance. By combining the thermal EoS, chemical compositions, and proportions of mantle minerals, we can now calculate the densities of the KLB-1 assemblages over the entire range of lower mantle conditions. Figure 3 compares the density profiles calculated for several K_D values with the PREM model [*Dziewonski and Anderson*, 1981]. The density profiles of KLB-1 peridotite through the lower mantle were calculated along the adiabatic geotherm of *Brown and Shankland* [1981]. First, we fixed the phase proportion to 77 wt% Mg-pv, 16 wt% ferropericlase and 7 wt% Ca-pv (63 mol%, 31 mol% and 5 mol%, respectively). Density profiles obtained for K_D from 0.47 to 1.25 are very close to each other represented by the shaded area (Figure 3). The difference between them does not exceed 0.1%. The fixed proportions are only consistent with K_D values between 0.64 and 0.76, according to mass balance calculations. For K_D values of 0.47 and 1.25, mass balance requires different phase proportions to match the pyrolite composition. For instance, a K_D value of 0.47 resulted in optimized phase proportions of 20 wt% ferropericlase, 73 wt% Mg-pv, and 7 wt% Ca-Pv, whereas a K_D value of 1.25 led to 13 wt% ferropericlase, 80 wt% Mg-pv, and 7 wt% Ca-Pv. These density profiles were plotted for comparison (Figure 3). It is clear that the calculated pyrolite density profiles deviate from PREM (Figure 3), too low at the uppermost part of the lower mantle and too high in the bottom of the mantle. The change in Fe-Mg partition coefficient between Mg-perovskite and ferropericlase does not change the trend.

4. Discussion and Conclusion

[10] If we want to match the measured density profile for a pyrolite mantle composition with PREM, the temperature at the top of the lower mantle has to be ~1500 K (±60 K for extreme K_D values) with a superadiabatic geotherm (~0.60 K/km through the lower mantle). This temperature is 400 K lower than expected at 660 km depth [e.g., *Hirose*, 2002] and the gradient is twice of the adiabatic geotherm gradient. The temperature at the 660 km depth is still under debate [*Frost*, 2008] due to inconsistent pressure calibration, but a temperature of 1500 K seems too low to be consistent with the melting generation in the mid-ocean ridge and hotspot volcanism.

[11] We have also examined the effect of iron by using composition dataset from *Irifune* [1994] where the iron bulk molar fraction is 0.116 with a K_D value of 0.75 (see Figure S5). We obtain a 0.42% higher density profile than that with an iron bulk molar fraction of 0.106 (Figure 3). The higher iron content would increase the temperature to

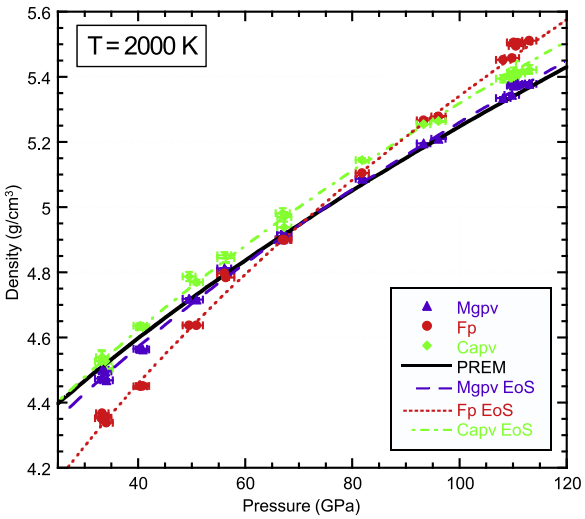

Figure 2. Pressure-density relationship of Mg-perovskite (triangles), Ca-perovskite (diamonds), and ferropericlase (circles) at 2000 K (±50 K). The PREM density profile is also plotted for comparison.

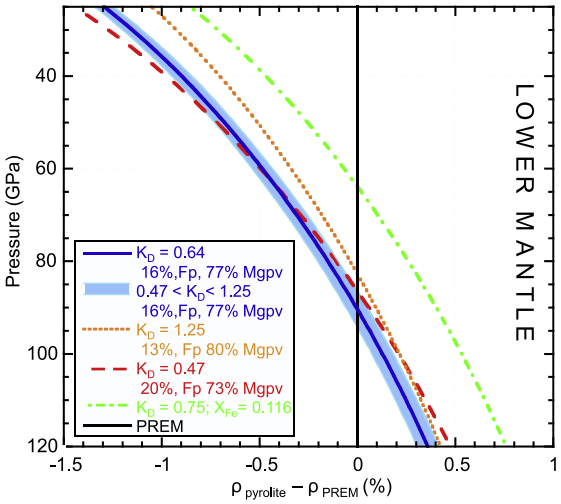

Figure 3. The difference between the measured pyrolite density and PREM as a function of pressure along a geotherm temperature profile [*Brown and Shankland*, 1981]. The blue profile is the density difference obtained using the phase compositions with a partition coefficient of 0.64 and phase proportions of 77 wt% Mg-perovskite, 16 wt% ferropericlase, and 7 wt% Ca-perovskite. The blue area represents the range of possible density profiles when applying different phase compositions (i.e. partition coefficients from 0.47 to 1.25 with fixed phase proportions). For extreme partition coefficients, these phase proportions are not correct in terms of mass balance. The orange dotted curve represents the density difference for K_D = 1.25 and the orange curve for K_D = 0.47, with the phase proportions given in the text. The effect of iron content (X_{Fe} = 0.116) on the density is shown by the green dashed-dotted curve.

1600 K at 660-km depth to match the PREM model, but it still requires a superadiabatic geotherm (0.7 K/km). The origin of the deviation of the measured density of pyrolitic mantle from PREM and its slope can be traced to the high-temperature density profile of ferropericlase which is much more compressible than the coexisting perovskites and mantle PREM (Figure 2). In the pyrolite model, the lower mantle would contain about 16 wt% ferropericlase which leads to the significant mismatch between the pyrolitic mantle density and PREM. Our data would be consistent with a perovskitic lower mantle on the basis of density argument. Differences between this study and previous studies on lower mantle properties can be attributed to the EoS of aluminum and iron-bearing Mg-perovskite, which shows lower bulk modulus and higher thermal parameters than pure Mg-perovskite. A perovskite dominated lower mantle is also supported by recent sound velocity measurements of $MgSiO_3$ perovskite [*Murakami et al.*, 2007].

[12] We have demonstrated that there is a deviation of the density profile of pyrolite from PREM in the lower mantle, particularly the mismatch of the slopes between the two profiles. The discrepancy cannot easily be resolved if we consider the uncertainties in the experimental data (e.g., 0.3% corresponding to an error of 1 GPa or 100 K at the top of the lower mantle) and PREM model (0.5%). It is even more difficult to reconcile the steeper slope of our density profile with that of PREM. If the pyrolite model represents the composition of the Earth's upper mantle, our experimental data imply that the upper and lower mantle must have different chemical compositions, i.e. a chemically stratified mantle, using PREM as a reference. In that case, the data favor a perovskite dominated, Si-enriched, lower mantle. Alternatively, the assumptions and uncertainties of PREM need to be re-evaluated, particularly in respect to the adiabaticity and the fit of the free-oscillation data [*Kennett*, 1998]. In any case, our pyrolite density profile provides the first experimental determination of density profile for a homogeneous lower mantle.

[13] **Acknowledgments.** This study was supported by the National Science Foundation (Geophysics grant to YF) and the Carnegie Institution of Washington. We thank Eiichi Takahashi for providing the KLB-1 sample. The experimental work was performed at GeoSoilEnviroCARS synchrotron beamline, supported by NSF, DOE, and the State of Illinois.

References

Badro, J., G. Fiquet, F. Guyot, J. Rueff, V. V. Struzhkin, G. Vanko, and G. Monaco (2003), Iron partitioning in Earth's mantle: Toward a deep lower mantle discontinuity, *Science*, *300*, 789–791.

Brown, J. M., and T. J. Shankland (1981), Thermodynamic parameters in the Earth as determined from seismic profiles, *Geophys. J. R. Astron. Soc.*, *66*, 579–596.

Dziewonski, A., and D. Anderson (1981), Preliminary Reference Earth Model, *Phys. Earth Planet. Inter.*, *25*, 297–356.

Fei, Y., A. Ricolleau, M. Frank, K. Mibe, G. Shen, and V. Prakapenka (2007a), Toward an internally consistent pressure scale, *Proc. Natl. Acad. Sci. U. S. A.*, *104*, 9182–9186, doi:10.1073/pnas.0609013104.

Fei, Y., L. Zhang, A. Corgne, H. Watson, A. Ricolleau, Y. Meng, and V. Prakapenka (2007b), Spin transition and equations of state of (Mg, Fe)O solid solutions, *Geophys. Res. Lett.*, *34*, L17307, doi:10.1029/2007GL030712.

Fiquet, G., A. Dewaele, D. Andrault, M. Kunz, and T. LeBihan (2000), Thermoelastic properties and crystal structure of $MgSiO_3$ perovskite at lower mantle pressure and temperature conditions, *Geophys. Res. Lett.*, *27*, 21–24.

Frost, D. J. (2008), The upper mantle and the transition zone, *Elements*, *4*, 171–176, doi:10.2113/GSELEMENTS.4.3.171.

Hirose, K. (2002), Phase transitions in pyrolitic mantle around 670-km depth: Implications for upwelling of plumes from the lower mantle, *J. Geophys. Res.*, *107*(B4), 2078, doi:10.1029/2001JB000597.

Irifune, T. (1994), Absence of an aluminous phase in the upper part of the Earth's lower mantle, *Nature*, *370*, 131–133.

Jackson, I., and S. Rigden (1996), Analysis of P-V-T data: Constraints on thermoelastic properties of high-pressure minerals, *Phys. Earth Planet. Inter.*, *96*, 85–112.

Kennett, B. L. N. (1998), On the density distribution within the Earth, *Geophys. J. Int.*, *132*, 374–382.

Kesson, S. E., J. D. Fitz Gerald, and J. M. Shelley (1998), Mineralogy and dynamics of a pyrolite lower mantle, *Nature*, *393*, 252–255.

Komabayashi, T., K. Hirose, N. Sata, Y. Ohishi, and L. S. Dubrovinsky (2007), Phase transition in $CaSiO_3$ perovskite, *Earth Planet. Sci. Lett.*, *260*, 564–569.

Lee, K. M., B. O'Neill, W. R. Panero, S. H. Shim, L. R. Benedetti, and R. Jeanloz (2004), Equations of state of the high-pressure phases of a natural peridotite and implications for the Earth's lower mantle, *Earth Planet. Sci. Lett.*, *223*, 381–393.

Mao, H. K., G. Chen, and R. J. Hemley (1997), Multivariable dependence of Fe-Mg partitioning in the lower mantle, *Science*, *278*, 2098–2100.

McDonough, W. F., and S. Sun (1995), The composition of the Earth, *Chem. Geol.*, *120*, 223–253.

Meng, Y., D. J. Weidner, and Y. Fei (1993), Deviatoric stress in a quasi-hydrostatic diamond anvil cell: Effect on the volume-based pressure calibration, *Geophys. Res. Lett.*, *20*, 1147–1150.

Murakami, M., K. Hirose, N. Sata, and Y. Ohishi (2005), Post-perovskite phase transition and mineral chemistry in the pyrolitic lowermost mantle, *Geophys. Res. Lett.*, *32*, L03304, doi:10.1029/2004GL021956.

Murakami, M., S. V. Sinogeikin, H. Hellwig, J. D. Bass, and J. Li (2007), Sound velocity of $MgSiO_3$ perovskite to Mbar pressure, *Earth Planet. Sci. Lett.*, *256*, 47–54.

Nishiyama, N., and T. Yagi (2003), Phase relation and mineral chemistry in pyrolite to 2200°C under the lower mantle pressures and implications for

dynamics of mantle plumes, *J. Geophys. Res.*, *108*(B5), 2255, doi:10.1029/2002JB002216.

Nishiyama, N., and T. Yagi (2007), Effect of incorporation of iron and aluminum on the thermoelastic properties of magnesium silicate perovskite, *Phys. Chem. Miner.*, *34*, 131–143.

O'Neill, B., and R. Jeanloz (1990), Experimental petrology of the lower mantle: A natural peridotite taken to 54 GPa, *Geophys. Res. Lett.*, *17*, 1477–1480.

Ringwood, A. E. (1975), *Composition and Petrology of the Earth's Mantle*, 618 pp., McGraw-Hill, New York.

Shen, G., M. L. Rivers, Y. Wang, and S. R. Sutton (2001), A laser heated diamond cell system at the Advanced Photon Source for in situ x-ray measurements at high pressure and temperature, *Rev. Sci. Instrum.*, *72*, 1273–1282.

Stacey, F. D. (1996), Thermoelasticity of (Mg, Fe)SiO_3 perovskite and a comparison with the lower mantle, *Phys. Earth Planet. Inter.*, *98*, 65–77.

Stixrude, L., R. J. Hemley, Y. Fei, and H. K. Mao (1992), Thermoelasticity of silicate perovskite and magnesiowustite and stratification of the Earth's mantle, *Science*, *257*, 1099–1101.

Takahashi, E. (1986), Melting of a dry peridotite KLB-1 up to 14 GPa: Implications on the origin of peridotite upper mantle, *J. Geophys. Res.*, *91*, 9367–9382.

Tsuchiya, T., R. M. Wentzcovitch, C. R. S. da Silva, and S. de Gironcoli (2006), Spin transition in magnesiowustite in Earth's lower mantle, *Phys. Rev. Lett.*, *96*, 198501.

Wang, Y., D. J. Weidner, and F. Guyot (1996), Thermal equation of state of $CaSiO_3$ perovskite, *J. Geophys. Res.*, *101*, 661–672.

Wood, B. J. (2000), Phase transformations and partitioning relations in peridotite under lower mantle conditions, *Earth Planet. Sci. Lett.*, *174*, 341–354.

A.-L. Auzende, G. Fiquet, and G. Morard, Institut de Physique du Globe de Paris, IMPMC, 140 rue de Lourmel, Paris F-75015, France.

E. Cottrell, L. Deng, Y. Fei, A. Ricolleau, H. Watson, and L. Zhang, Geophysical Laboratory, Carnegie Institution of Washington, 5251 Broad Branch Road, NW, Washington, DC 20015, USA. (a.ricolleau@gl.ciw.edu)

V. Prakapenka, Center for Advanced Radiation Sources, University of Chicago, 9700 South Cass Avenue, Argonne, IL 60439, USA.

M. Roskosz, Laboratoire de Structure et Proprietes de l'Etat Solide, Université des Sciences et Techniques de Lille, Bâtiment C6, Villeneuve d'Ascq F-59655, France.